https://doi.org/10.1016/j.ejps.2019.105047

European Journal of Pharmaceutical Sciences
Volume 139, 1 November 2019, 105047

TSPO-targeted NIR-fluorescent ultra-small iron oxide nanoparticles for glioblastoma imaging

NunzioDenora[ab1] ChaedongLee[c1] Rosa MariaIacobazzi[d] Ji YoungChoi[ce] In HoSong[e] Jung SunYoo[f] YuanzhePiao[cg] AntonioLopalco[a] FrancescoLeonetti[a] Byung ChulLee[eg] Sang EunKim[ceg]

[a] Department of Pharmacy – Drug Sciences, University of Bari "Aldo Moro", Bari 70125, Italy

[b] Institute for Physical and Chemical Processes (IPCF)-CNR, SS Bari, Via Orabona, St. 4, 70125 Bari, Italy

[c] Department of Transdisciplinary Studies, Graduate School of Convergence Science and Technology, Seoul National University, Seoul 16229, Republic of Korea

[d] IRCCS Istituto Tumori "Giovanni Paolo II" of Bari, 70124 Bari, Italy

[e] Department of Nuclear Medicine, Seoul National University College of Medicine, Seoul National University Bundang Hospital, Seongnam 13620, Republic of Korea

[f] Department of Health Technology and Informatics, The Hong Kong Polytechnic University, Hong Kong Special Administrative Region

[g] Advanced Institutes of Convergence Technology, Suwon 16229, Republic of Korea

Received 22 February 2019, Revised 15 July 2019, Accepted 15 August 2019, Available online 15 August 2019.

Abstract

The translocator protein 18 kDa (TSPO) is mainly located in outer membrane of mitochondria and results highly expressed in a variety of tumor including breast, colon, prostate, ovarian and brain (such as glioblastoma). Glioblastoma multiforme (GBM) is the most common and lethal type of primary brain tumor. Although GBM patients had currently available therapies, the median survival is <14 months. Complete surgical resection of GBM is critical to improve GBM treatment. In this study, we performed the one-step synthesis of water-dispersible ultra-small iron oxide nanoparticles (USPIONs) and combine them with an imidazopyridine based TSPO ligand and a fluorescent dye. The optical and structural characteristics of TSPO targeted-USPIONs were properly evaluated at each step of preparation demonstrating

the high colloidal stability in physiological media and the ability to preserve the relevant optical properties in the NIR region. The cellular uptake in TSPO expressing cells was assessed by confocal microscopy. The TSPO selectivity was confirmed *in vivo* by competition studies with the TSPO ligand PK 11195. *In vivo* fluorescence imaging of U87-MG xenograft models were performed to highlight the great potential of the new NIR imaging nanosystem for diagnosis and successful delineation of GBM.

Graphical abstract

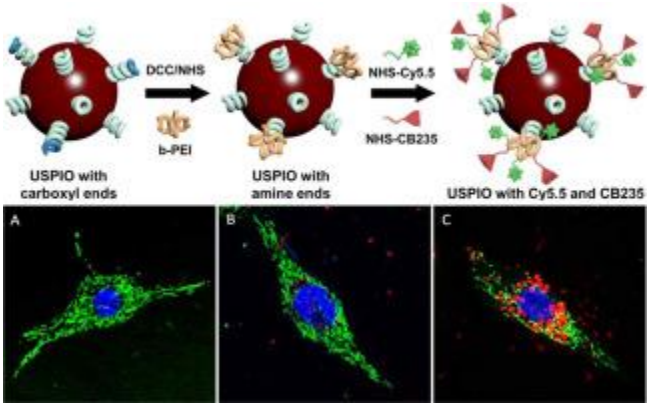

Keywords

Glioblastoma multiforme
NIR imaging
Mitochondrial targeting
TSPO
USPIONs

1. Introduction

Among the intracellular targets the translocator protein 18 kDa (TSPO) is one of the most investigated and promising, as it appears to be over-expressed in some types of cancers, including breast, colon, prostate, ovarian and brain (such as glioblastoma) compared to healthy tissues. In particular, TSPO is located in the outer membrane of mitochondria as a component of a multi-proteic complex named mitochondrial

permeability transition pore (MPTP), involved in various cellular functions including cholesterol transport, steroid hormone synthesis, mitochondrial respiration, permeability transition pore opening, programmed cell death (apoptosis) and proliferation (Iacobazzi et al., 2017b; Lopalco et al., 2018; Mangiatordi et al., 2017; Piccinonna et al., 2013; Savino et al., 2016). TSPO has therefore become an attractive subcellular target for both the early detection of disease states involving its overexpression and the selective mitochondrial drug delivery (Perrone et al., 2016). The amount of structurally different TSPO ligands examined has increased over time revealing a broad spectrum of actions, such as anti-steroidogenic or pro-apoptotic effects potentially useful for cancers therapy (Iacobazzi et al., 2017b). In recent times new PET imaging probes and various metal-based complexes targeting the TSPO have been projected to monitor the TSPO expression in neuro pathological diseases such as neuroinflammation and tumors (Choi et al., 2016; Denora et al., 2017; Iacobazzi et al., 2017a; Laquintana et al., 2016; Midzak et al., 2015; Piccinonna et al., 2012). Specifically, glioblastoma multiforme (GBM) is the most common and deadly type of primary brain cancer. Although GBM patients have currently available therapies, including radiation and chemotherapy with temozolomide, the median survival is <14 months after diagnosis mainly due to the occurrence of resistance phenomena (Stupp et al., 2009). Complete surgical resection of GBM is critical to improve GBM treatment. Therefore, the discovery of new targets for early diagnosis and GBM therapy is becoming increasingly necessary (Elkamhawy et al., 2015). For an advanced diagnosis of tumors, the essentials characteristics of the imaging probes are high affinity for the target sites, selective cellular internalization, and an *in vivo* high stability. In addition, such probes are required to be nontoxic and easy to prepare. Since TSPO is selectively over expressed in the brains of the GBM patients (Elkamhawy et al., 2015), TSPO ligands can be exploited as targeting moiety for the early diagnosis and successful delineation of GBM by means of *in vivo* fluorescence and nuclear imaging, as well as for the glioblastoma therapy. In addition to the identification of new targets for GBM a winning strategy could be the use of appropriately engineered nanoparticles systems able to selectively target the glioblastoma cells. This would overcome the limits of the classical molecules currently used for the diagnosis and therapy of brain cancers, including the difficulty of crossing the blood-brain barrier (BBB). Moreover, approaches to increase the

delivery of pharmacological active molecules to the brain tissue without opening of the brain vascular system are urgently needed and for this purpose nanoparticles represent an effective opportunity to reach this target, in particular in cerebral tumors. Ultra-small superparamagnetic iron oxide nanoparticles (USPIO NPs) are particularly promising since their magnetic properties increase the number of potential applications in the biomedical area, including drug delivery, thermotherapy, imaging and detection of tumor. Their potential to cross biological barriers, including the BBB and the blood−brain tumor barrier (BBTB) have been recently confirmed (Cassano et al., 2017; Halamoda Kenzaoui et al., 2013; Lopalco et al., 2015) using an *in vitro* model representative of the endothelial-glioblastoma tumor barrier. They demonstrated that USPIO NPs can be translocated from endothelial cells to glioblastoma cells. The selection of the surface molecules for iron oxide nanoparticles is crucial for biological uses, since the good stability in physiological buffer, the biocompatibility, and the prevention of the nonspecific interaction with a cell, are strictly dependent from this issue. In particular, low molecular weight polyethyleneglycol (PEG) has been paid a lot of attention as a potential organic surface molecule from a biomedical point of view. PEG anchored on the surface of NPs leads to decrease nonspecific binding with cells and enhances viability and stability by retaining a helical conformation of the crystalline state in water (Depalo et al., 2017). For these reasons we decided to prepare ultra-small PEGylated water-dispersible iron oxide nanoparticles (USPIONs) following the one step synthesis method previously reported (Yang et al., 2014). In particular we projected and realized iron oxide nanoparticles surface grafted with an imidazopyridine based TSPO ligand properly synthesized in our laboratory, as a targeting moiety (Denora et al., 2013, Denora et al., 2008), and with a near infrared (NIR) emitting fluorescent dye in order to perform *in vivo* fluorescence and nuclear imaging for the diagnosis and thesuccessful delineation of GBM. The use of targeted nanoplatform-based probes aims to extend plasma half-lives, thus increasing *in vivo* stability and targeting efficiency. Several TSPO targeted nanoparticles have been yet proposed as potential and efficacious fluorescent agents for visualization of trafficking inside cell and for *in vivo* imaging (Denora et al., 2013; Fanizza et al., 2016a; Lopalco and Denora, 2018). Optical imaging consents several advantages, including accurate sensitivity, non-invasive procedure, and a reasonable cost of the instrument for the detection.

Remarkably, the use of fluorescent probes emitting in the near-infrared region (NIR, 700–1100 nm), can enhance the signal-to-noise ratio in *in vivo* technique of optical imaging. In the NIR region, autofluorescence and scattering by biological tissues are minimal, therefore NIR probes are expected to result in high resolution and deep penetration images (Depalo et al., 2017a).

The novel synthesized TSPO targeted-NIR-fluorescent ultra-small iron oxide nanoparticles have been thoroughly investigated, assessing the NIR emitting properties upon surface functionalization with TSPO ligand, and elucidating the morphology, size, colloidal stability of the nano-object in each step of preparation. Various techniques have been applied for the characterization of this system, such as transmission electron microscopy (TEM), dynamic light scattering (DLS) and fluorescence spectroscopy. *In vitro* toxicity study of TSPO-targeted nanoparticles was performed in U937 (human histiocytic lymphoma cell), which is one of the TSPO-overexpressed cell lines. The uptake experiments *in vitro* were conducted by means of confocal microscopy in human glioblastoma U87-MG and human prostate PC3 cancer cell lines in live mode and after immunocytofluorescent staining in PC3 and in human fibroblast CCD-986sk fixed cells. Moreover, the correlation between inflammatory responses and TSPO expression at a cellular level was evaluated. The efficacy of the USPIOs-TSPO targeted *in vivo* as a tool for fluorescence imaging of GBM was assessed in 6-week-old male Balb/c athymic mice. Competition studies were also performed *in vivo* using the selective TSPO ligand PK 11195.

2. Materials and methods

Ethylenediamine, branched polyethyleneimine (b-PEI, Mw ~800), dicyclohexylcarbodiimide (DCC), *N*-dydroxysuccinimide (NHS) and phosphate buffered saline (PBS) tablets were from Sigma Aldrich. Ferric nitrate nonahydrate ($Fe(NO_3)_3 \cdot 9H_2O$), ethanol, polyethyleneglycol (PEG, Mw ~600), dimethylsulfoxide (DMSO) and diethyl ether were purchased from Samchun Chemical (South Korea). Cyanine 5.5 dye (Flamma® 675 NHS ester) was bought from BioActs (South Korea). Other reagents were purchased from Sigma-Aldrich and Tokyo Chemical Industry Co., Ltd. (TCI). All the reagents were used without further purification and aqueous solutions were prepared using high purity deionized water (18.2 MΩ). ^{1}H and ^{13}C

NMR spectra were recorded on a Varian at 400-MR (400 MHz) spectrometer (Agilent Technologies, USA). Chemical shifts were reported in parts per million (ppm, δ units). Electrospray mass spectrometry (ESI-MS) was performed on a LC/MS spectrometer (Agilent 6130 Series, Agilent Technologies, USA). HPLC was carried out on a Dong-il Shimadzu Corp (Japan). Separation Products System equipped with a semi-preparative column (Waters, Xterra RP-C18, 10 μm, 10 × 250 mm) and equipped with a UV detector (wavelength set at 254 nm). HPLC-grade solvents (*J*. T. Baker, USA) were used for HPLC purification after filtering with membrane filter (Whatman, 0.22 μm, USA). The HPLC eluent started with 65% acetonitrile and 35% water over 25 min at a flow rate of 4 mL/min. A fluorometer (Fluorolog 3, HORIBA Jobin-Yvon) was used for the quantitative analysis of the fluorescent dyes bound to the particles.

2.1. Cell lines

U87-MG (human malignant glioblastoma cell), PC-3 (human prostate cancer cell), U937 (human histiocytic lymphoma cell) and CCD-986sk (human fibroblast) were distributed from Korean Cell Line Bank (Seoul, Korea) and grown in Dulbecco's Modified Eagle's Medium (DMEM, SH30243.01; GE Healthcare, USA), Roswell Park Memorial Institute 1640 Medium (RPMI-1640, SH30027.01; GE Healthcare, USA) and Iscove's Modified Dulbecco's Medium (IMDM, SH30228.01; GE Healthcare, USA) respectively with 10% heat-activated fetal bovine serum (FBS, SH30919.03; GE Healthcare, USA) and 1% penicillin-streptomycin (15070-063; Life Technologies, USA). Cells were cultured at 37 °C in a humidified 5% CO_2 incubator.

2.2. Synthesis of CB235-NHS

To a solution of 2-(4-(6,8-dichloro-3-(2-(dipropylamino)-2-oxoethyl)imidazo[1,2-*a*]pyridin-2-yl)phenoxy)acetic acid (CB235) (50 mg, 0.10 mmol) in dichloromethane (5 mL) was added NHS, (14 mg, 0.12 mmol) and DCC (25 mg, 0.12 mmol). The reaction mixture was stirred at room temperature for 4 h. The solvent was removed under reduced pressure and then the reaction mixture was dissolved in acetonitrile:water = 65:35 (v/v). The product was separated by a semi-preparative HPLC system. The fraction of CB235-NHS was collected at 7.0 min as a white

solid; ^{1}H NMR (400 MHz, $CDCl_3$) δ 8.29 (s, 1H), 7.63 (d, J = 8.8 Hz, 2H), 7.28 (s, 1H), 7.07 (d, J = 9.2 Hz, 2H), 5.02 (s, 2H), 4.05(s, 2H), 3.30 (t, J = 7.8 Hz, 2H), 3.11 (t, J = 7.8 Hz, 2H), 2.87 (s, 4H), 1.56–1.46 (m, 4H), 0.88–0.84 (m, 3H), 0.74–0.70 (m, 3H); ^{13}C NMR (100 MHz, $CDCl_3$) δ 170.5, 167.1, 158.7, 140.6, 130.6, 125.9, 122.6, 121.7, 120.2, 117.3, 114.9, 65.5, 50.0, 48.2, 31.0, 30.0, 22.2, 20.9, 11.3, 11.1; MS (ESI) *m*/*z* 575.1 ($M + H^+$, 100%) 577.1 (60%) 576.1 (30%), 578.1 (20%), 579.1 (11%); HRMS (ESI) *m*/*z* $C_{27}H_{29}O_6N_4Cl_2$ calcd: 575.1459; found: 575.1488.

2.3. One step synthesis of water-dispersible ultra-small iron oxide nanoparticles (USPIONs)

The USPIONs in this research were reproduced following the previously reported method (Yang et al., 2014). Typically, 1 mmol of ferric nitrate nonahydrate and 20 mmol of PEG600 were transferred to 50 mL three-neck round bottom flask and degassed under 95 °C for 1 h. The color of the solution gradually changed to a deep reddish-brown color as it was heated. Then, the mixed solution was heated at 265 °C for 30 min to synthesize magnetite nanocrystals. A portion of the solution was mixed with a mixture of ethanol and ether, and then purified by centrifugation. The procedure was repeated three times, and the purified nanoparticles were dispersed in the desired solvent and stored.

2.4. Surface functionalization of USPIONs with branched polyethyleneimine (b-PEI)

As mentioned in the previous paper (Yang et al., 2014), since the iron oxide nanoparticles synthesized by this method have a carboxyl group on the surface, in this study, the surface functionalization was processed through amide bonding formation. The purified nanoparticles (~8 mg) were redispersed in 2 mL of DMSO, and each 1 mL of DCC and NHS solution (0.1 M in DMSO) was added. After shaking for 30 min, 1 mL of b-PEI solution (1 wt% in DMSO) was added to induce the reaction with NHS on the surface of the nanoparticles and the mixture was shaken for 4 h. Again, the nanoparticles were purified by centrifugation with a mixture of ethanol and ether and redispersed in ethanol for the next procedure.

2.5. Fluorescence labeling and TSPO-target ligand conjugation

Cyanine 5.5, a near-infrared fluorescent dye, was introduced on the surface of nanoparticles to reduce overlap of spectral absorbance by the iron oxide nanoparticles and to obtain a strong fluorescence image from the body. Both fluorescent dye and a CB-235 ligand, which had been pre-NHS-esterified at the end, were prepared and applied to the nanoparticles to facilitate attachment to the amine functional groups of the nanoparticles. 0.5 mmol of each was dissolved in 1 mL of ethanol and then added to an amine-functionalized iron oxide nanoparticle previously dispersed in 2 mL of ethanol, followed by shaking for 4 h. Unbound molecules were repeatedly centrifuged in the same manner as described above, and the nanoparticles were finally dispersed in a PBS solution for *in vivo* experiments. In order to remove trace amounts of residual ether, the solution was purified through dialysis and prepared at a concentration of 1 mg Fe/mL.

2.6. *In vitro* studies

2.6.1. TSPO expression levels

Relative expression levels of TSPO in four cell lines were determined by flow cytometry (Iacobazzi et al., 2017). The corresponding histoghrams are reported in Fig. 4a.

2.6.2. *In vitro* toxicity test

To evaluated the cytotoxic effect of the USPIONs, various Fe concentration (0, 15, 30 and 60 μg/mL) of the USPIONs were tested to four different cell lines (U87-MG and PC3 are the TSPO-positve cell lines; U937 and CCD-986sk are the TSPO-native cell lines). Cells were cultured in a 96-well plate with 5.0×10^3 cells per well. After incubating for 2, 4, 8 and 24 h, 20 μL of CellTiter 96 Aqueous assay reagent (Promega) were added into all wells according to the manufacturer's protocol. The plates were incubated for 1 h and the formazan products were measured by absorbance at 490 nm using a microplate reader.

2.7. *In vitro* cellular uptake study

Cells (U87-MG and PC3) were seeded in 10 mm-cover glass bottom dish as known as confocal dish at a density of 5×10^4 24 h before *in vitro* uptake study. Nanoparticles were added with serum containing media to the cells at concentration 20 μg/mL at 37 °C for 4 h. In addition, inhibitory experiments using PK 11195 were performed *in vitro* to prove the specificity of TSPO-targeted nanoparticles. Thus, U87-MG cells were treated with the combination nanoparticles (20 μg/mL) and PK 11195 (2 mg/mL) at 37 °C for 4 h. For cell nucleus and mitochondria staining, cells were soaked with 1× phosphate buffered saline (PBS) gently so as not to be detached. Shortly afterward, cells were incubated with Hoechst (H3570, 1:500; Life Technologies, USA) in serum free medium at 37 °C for 20 min and then with 2 μM MitoTracker™ Green FM (M7514; Life Technologies, USA) under same condition as Hoechst staining for 10 min. Cells were visualized by A1 Rsi Confocal Laser Scanning Microscope (Nikon, Japan) with X60 magnification.

The overlap coefficients were calculated (Fanizza et al., 2016b), according to Manders through the following equation:r=∑iS1i · S2i∑iS1i2 · ∑iS2i2;0≤r≤1where S_{1i} and S_{2i} represent signal intensity of pixels in the channel 1 (red) and in the channel 2 (green). Co-localization analysis was performed by using software ImageJ. Moreover, cellular uptake of targeted and not targeted NPs in U87-MG and PC3 cells was evaluated by measuring iron content through ICP-MS analysis (Depalo et al., 2017b). Cells were seeded in 60 mm tissue culture dishes at a density of 500,000 cells/dish and incubated at 37 °C in a humidified atmosphere with 5% CO_2. After 24 h, the culture medium was replaced with 3 mL of medium containing TSPO-targeted and not targeted nanoparticles at concentration 20 μg/mL and incubated for 4 and 24 h. After incubation, the cell monolayer was washed twice with ice-cold PBS and then digested with 2 mL of a HNO_3 (67%)/H_2O_2 (30%), 1:1 (v/v), solution for 4 h at 60 °C in a stove. The iron content was determined by ICP-MS with a Varian 820-MS ICP mass spectrometer.

2.8. *In vitro* immunocytofluorescent staining study

All the cells (PC3 and CCD-986sk) were seeded in 10 mm-cover glass bottom dish at a density of 5×10^4, 24 h before immunocytofluorescent staining just the same as cellular uptake study. Nanoparticles were treated with serum containing media to the

cells by 20 μg/mL at 37 °C for 4 h. The cells were fixed with 4% paraformaldehyde (PFA) for 20 min and then rinsed with PBS. After that, 0.2% Triton X-100 was treated into the cells for 15 min. For blocking of endogenous activity, the cells were placed with 4% bovine serum albumin (BSA) overnight at 4 °C. These blocked cells were then incubated with PBR antibody (ab109497, 1:200; Abcam, Cambridge, UK) as a primary antibody in serum free medium overnight at 4 °C. After gently washing, a rabbit secondary antibody, Alexa fluor 488 (A11034, 1:1000; Life Technologies, CA, USA), was added into the cells and the cells were incubated for 1 h at 20–25 °C. Nuclear DNA was stained with Hoechst for 10 min. In addition, 1 mg/mL LPS was added into the cells overnight before the treatment of TSPO-targeted nanoparticles Afterward, immunocytofluorescent staining was performed exactly same as above to assess the relationship between inflammatory responses and TSPO expression at a cellular level. Stained cells were visualized by A1 Rsi Confocal Laser Scanning Microscope (Nikon, Japan) with X60 magnification.

2.9. Animal models

6-week-old male Balb/c athymic mice were used in this *in vivo* experiment and those mice were purchased from Orient Biotech (Seoul, Korea). The animals were anesthetized with 2% isoflurane gas and 1×10^7 U87-MG cells with cold PBS were inoculated into forelimb armpit of mice (n = 15) subcutaneously with a sterile 26-gauge needle. After 2 weeks, U87-MG xenograft models were obtained for imaging experiment. All the animals had been administered on a regular diet and all *in vivo* experiments were performed in accordance with the guidelines by Institutional Animal Care and Use Committee (IACUC) and Seoul National University Animal Care.

2.10. *In vivo* fluorescence imaging

Animals were anesthetized by 2% isoflurane gas and 200 μg nanoparticles were administered intravenously with insulin syringe. *In vivo* fluorescence images were acquired at 30 min, 1 h, 4 h, 8 h and 24 h using *In Vivo* Imaging System (IVIS Lumina XRMS, CLS136340; Perkin Elmer, USA) with the indicated wavelength (excitation: 660 nm, emission: 710 nm). For blocking test, additional fluorescence imaging was

performed with the same protocol at 10 min after injection of 200 μg PK 11195 to examine selective displacement of the nanoparticle to TSPO. Mice were kept alive and maintained body temperature at 37 °C during the imaging experiment. All images were analyzed by ImageJ open source image processing software in terms of calculation of target-to-background (TBR).

3. Results and discussion

3.1. Synthesis and characterization of the TSPO ligand

Before synthesized TSPO targeted nanoparticle, we prepared the TSPO ligand. This ligand contained a 2-phenylimidazo[1,2-*a*]pyridine acetamide structure was reported in our previous studies (Denora et al., 2013, Denora et al., 2008). Especially, 2-(4-(6,8-dichloro-3-(2-(dipropylamino)-2-oxoethyl)imidazo[1,2-*a*]pyridin-2-yl)phenoxy)acetic acid (CB235) has a high affinity and selectivity for TSPO as demonstrated by (Denora et al., 2013; Fanizza et al., 2016a; Midzak et al., 2015). In particular, these authors in order to assess the affinity and selectivity of CB235 *versus* TSPO performed a receptor binding assay for CBR (central-type benzodiazepine receptor) and TSPO from rat cerebral cortex. PK 11195 (a selective ligand for TSPO) and flunitrazepam (a selective ligand for CBR) were used for comparison. CB235 displayed high affinity for TSPO and low for CBR, infact the reported inhibitory concentration values (IC_{50}) were 2.74 nM and $>10^5$ nM for TSPO and CBR, respectively. In order to simply conjugate with iron oxide nanoparticle and CB235, the CB235-NHS was synthesized according to the scheme reported in Fig. 1. The TSPO ligand CB235 was treated in dichloromethane at room temperature with DCC and NHS. The desired compound was obtained in good yield (60%) and revealed a HPLC retention time of 7 min. The CB235-NHS was characterized by ^{1}H NMR and ^{13}C NMR spectroscopy and by HRMS (ESI).

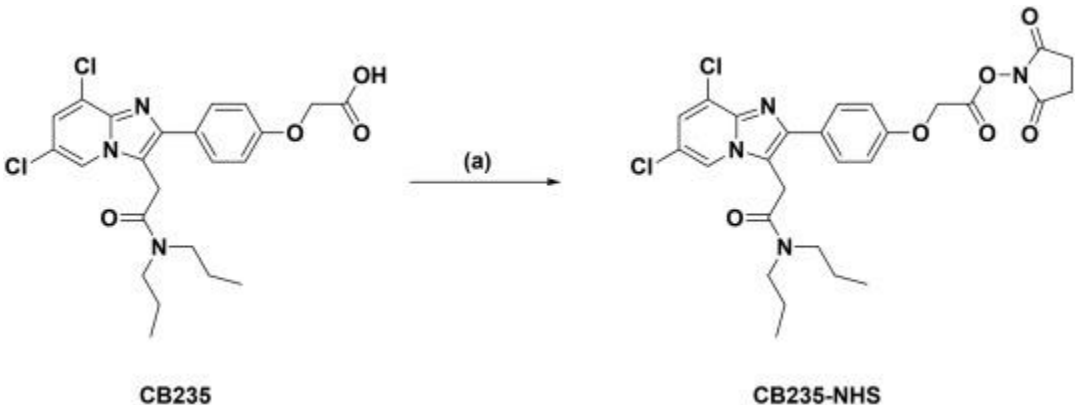

Fig. 1. Synthesis of TSPO ligand: (a) NHS, DCC, DCM, r.t., 4 h.

3.2. Synthesis and characterization of USPIO

The USPIO nanoparticles were synthesized using PEG as a solvent according to previously reported method, purified by centrifugation, and then functionalized as shown in Fig. 2a. Some carboxyl groups on the surface of the synthesized USPIO were allowed to bind the amine linker through a DCC/NHS coupling process, and then branched PEI (b-PEI, MW ~600) was introduced to expand the reaction site. Considering the solubility of Cyanine 5.5 (Cy5.5) and CB235, USPIO activated on the surface of the amine was dispersed in ethanol and used in the next reaction. Cy5.5 dye and CB235 ligand with NHS end were bound with simple stirring at room temperature. In this study, Cy 5.5, the near infrared fluorescent dye, was combined to minimize spectral overlap with iron oxide nanoparticles. By comparing the fluorescence intensities according to the concentration of each of the fluorescent dyes and nanoparticles using a fluorometer, quantitative analysis of the fluorescent dyes bound to the particles was performed. The results showed that about 722.9 nmol of fluorescent dye was bound per mg of nanoparticles. In case of the bifunctionally modified with TSPO ligand and the fluorescent dye at the same time, each moiety was fed in ratio of 1:1, thus it was predicted that they were bound by about 361.4 nmol for each 1 mg of the nanoparticles. The modified USPIO was observed to have an average diameter of about 5.57 nm through transmission electron microscopy, as shown in Fig. 2b and c. A comparison of the hydrodynamic size of pristine USPIO and modified USPIO through DLS analysis showed an increase of about 2.6 nm. As a result, it was confirmed that nanoparticles aggregation did not occur during the functionalization

process and the added molecules were successfully introduced to the surface of USPIO as we expected.

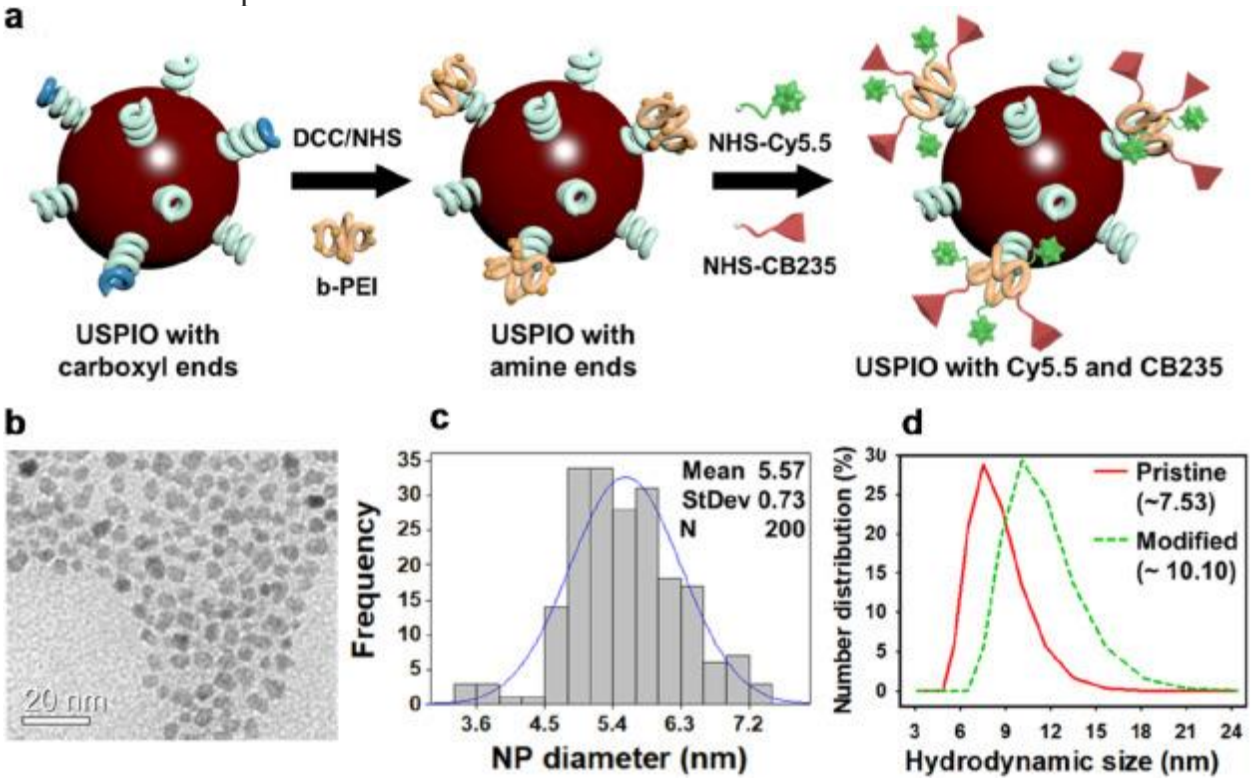

Fig. 2. (a) Schematic representation of Cy 5.5 and CB235 labeling process for USPIO. (b) TEM image of modified USPIO and (c) their size distribution histogram. (d) Hydrodynamic size change between the pristine USPIO and modified USPIO, measured by using DLS.

To verify the effect of the intermediate amine linker used for the introduction of fluorescent dyes, we compared pristine USPIO with two USPIO obtained using EDA and b-PEI as linkers, respectively. As shown in Fig. 3a, the darkest green color was observed in b-PEI, and fluorescence intensity was compared with that of EDA (Fig. 3b). This suggests that b-PEI, which is introduced to bind more TSPO target ligands and fluorescent dyes, acts as an effective linker as expected. In addition, we evaluated the hydrodynamic size of nanoparticles dispersed in 0.01–0.1 M PBS for 1 month to assess the dispersion stability of modified USPIO prior to *in vitro* and *in vivo* studies (Fig. 3c). The hydrodynamic size was slightly larger in the 0.1 M PBS which was 10 times thicker than the isotonic solution, but the USPIO was found to be dispersed well for a month without noticeable aggregation.

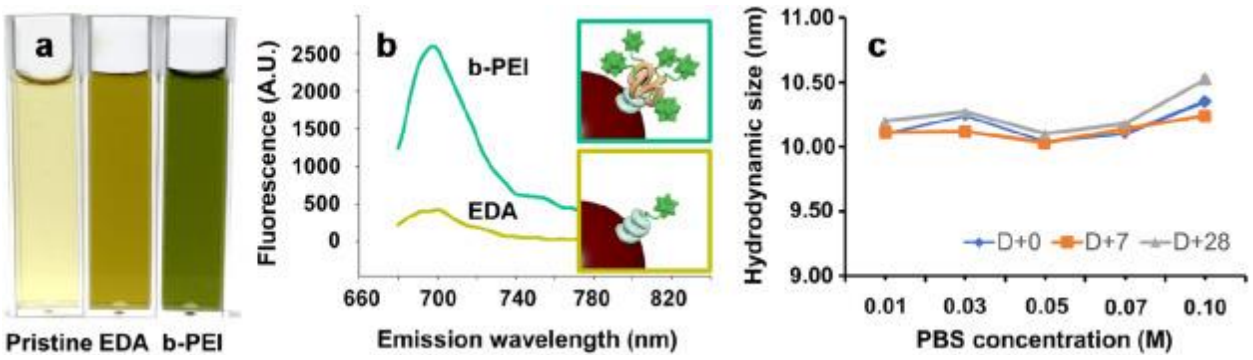

Fig. 3. (a) Comparison of USPIO solutions by color and (b) fluorescence intensity according to linker amines. (c) The change of the hydrodynamic size by 1-month DLS analysis.

3.3. *In vitro* studies

First of all, the relative expression levels of TSPO in four different cell lines were determined by flow cytometry (Fig. 4a). In particular, U87-MG (Mean Fluorescence Intensity (MFI) = 112.0) and PC-3 (MFI = 63.9) cell lines expressed a relatively high level of TSPO. For U937 (MFI = 10.1) and CCD-98Sk (MFI = 8.8) cell lines, TSPO expression was not detected. *In vitro* studies were carried out aimed first to assess the cytotoxicity of the nanosystem and subsequently its ability to reach the intracellular target site on the panel of cell lines over-expressing the TSPO receptor, namely U87-MG and PC3. CCD-986sk and U937 were used as a negative model in the uptake experiments. In these experiments water well-dispersed iron oxide nanoparticle with Cy5.5 and TSPO targeting ligand (10.10 nm) were used as TSPO targeted nanoparticle while water well-dispersed iron oxide nanoparticle with Cy5.5 (7.53 nm) were used as control nanoparticles.

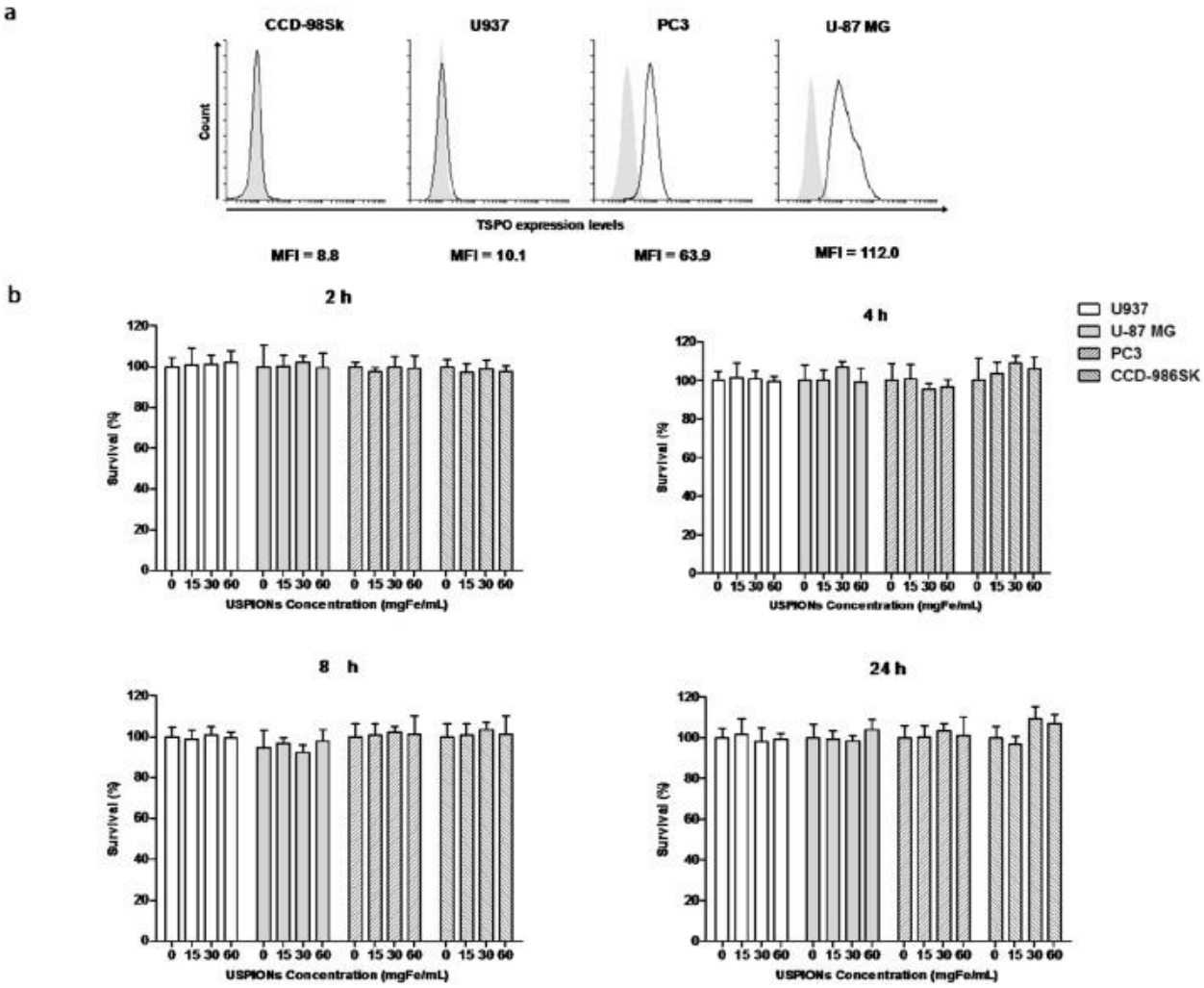

Fig. 4. (a) TSPO expression levels in U937, U87-MG, PC3 and CCD-986sk determined by flow cytometry; (b) cell viability of four different cell lines (U937, U87-MG, PC3 and CCD-986sk) after treatment with TSPO targeted nanoparticles in different Fe concentrations (0, 15, 30 and 60 μg/mL) at different time points (2, 4, 8, and 24 h).

3.3.1. *In vitro* toxicity

The toxicity of TSPO-targeted nanoparticles and of control nanoparticles (data not shown) was evaluated in all the above mentioned cell lines. The % cell viability after incubation with TSPO-nanoparticles for 2, 4, 8 and 24 h was determined by MTS assay and results are presented in Fig. 4b. As evidenced in the histograms the TSPO targeted nanoparticles did not affect the cell proliferation neither in terms of concentration nor of time exposure. This can support the idea that this new targeted imaging nanosystem will be not cytotoxic for a biomedical use.

3.3.2. *In vitro* cellular uptake study

The uptake of TSPO targeted nanoparticles was evaluated in two different cell lines overexpressing the TSPO, U87-MG and PC3, and in a negative model, namely the CCD-986sk human fibroblast cells. In particular, the analysis was conducted by means of confocal microscopy in live mode in U87-MG and PC3 cells (Fig. 5, Fig. 6, respectively) and after immunocytofluorescent staining in PC3 and in human fibroblast CCD-986sk fixed cells (Fig. 7). Confocal microscope images obtained after incubation of U87-MG (Fig. 5b and c) and PC3 (Fig. 6b and c) cells with TSPO targeted nanoparticles at increasing dose show clearly a comparable increase of the orange merging areas in the mitochondrial region compared with the images obtained for U87-MG cells (Fig. 5a) and PC3 cells (Fig. 6a) treated with control nanoparticles. The Manders' overlap coefficients, calculated for non-targeted and targeted nanoparticles, were 0.07 and 0.29 for U87-MG cells, 0.02 and 0.15 in PC3 cells. The higher Manders coefficient value measured for the TSPO-targeted NPs confirms the co-localization of the green and red detection channel, which are the green mitochondrial marker and the red targeted-nanoparticles, respectively. This co-localization confirms the ability of TSPO targeted nanoparticles to recognize the mitochondrial target TSPO. In addition, inhibitory experiments using PK 11195 were performed in the TSPO overexpressing cell line U87-MG to prove the specificity of TSPO-targeted nanoparticles. In Fig. 5d the confocal microscopy images obtained after the inhibitory experiment show a reduction of overlapped areas, confirming the competition of TSPO targeted nanoparticles with PK 11195 for the same receptor binding site.

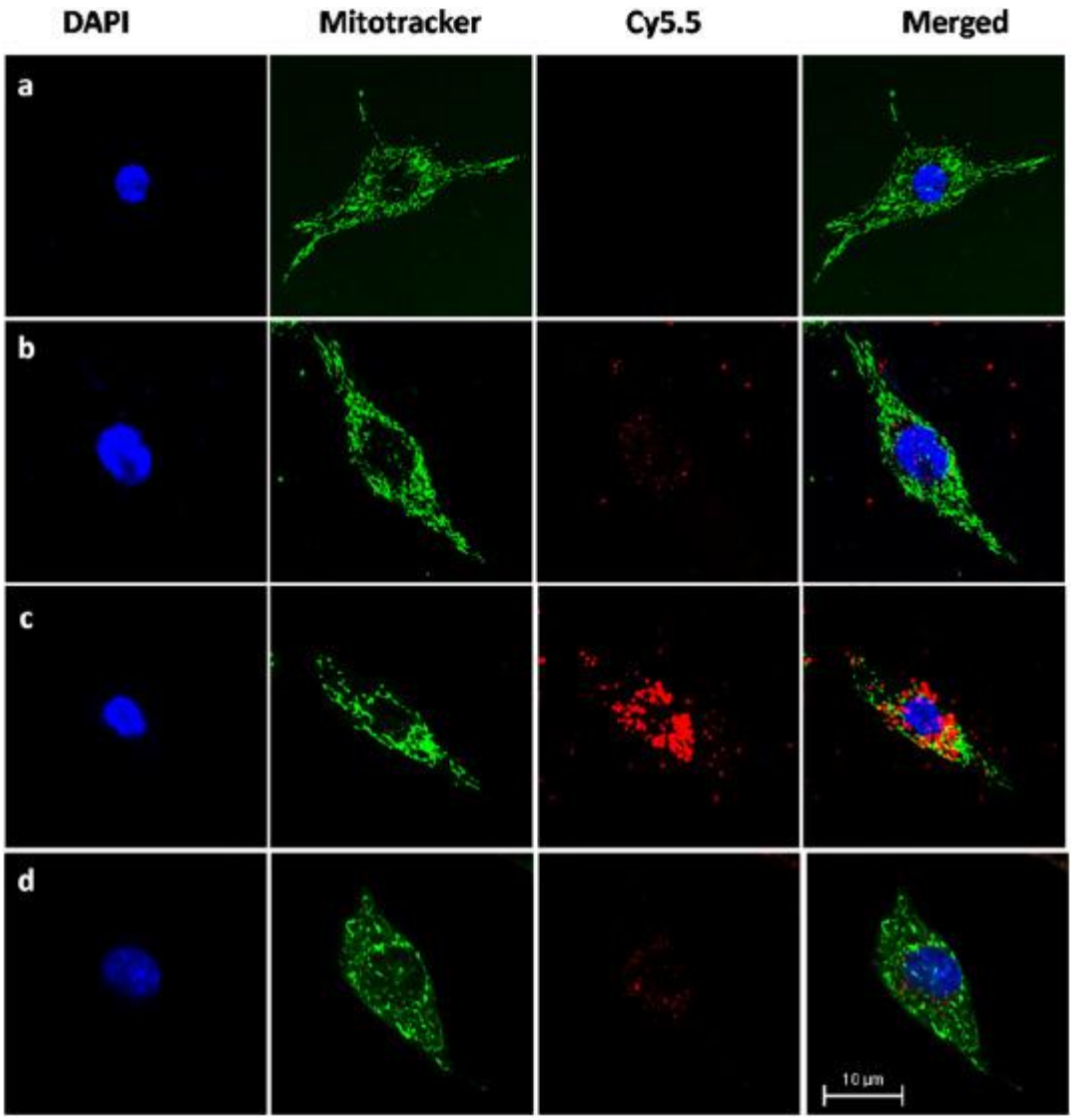

Fig. 5. Confocal microscope images of human glioblastoma U87-MG. (a) Control nanoparticles; (b) 10 µg/mL TSPO targeted nanoparticles; (c) 20 µg/mL TSPO targeted nanoparticles; (d) 20 µg/mL TSPO targeted nanoparticles in the presence of PK 11195 (2 mg/mL). Blue: nucleus (DAPI), Green: mitochondria (MitoTracker™ Green FM), Red: TSPO targeted nanoparticles (Cy5.5).

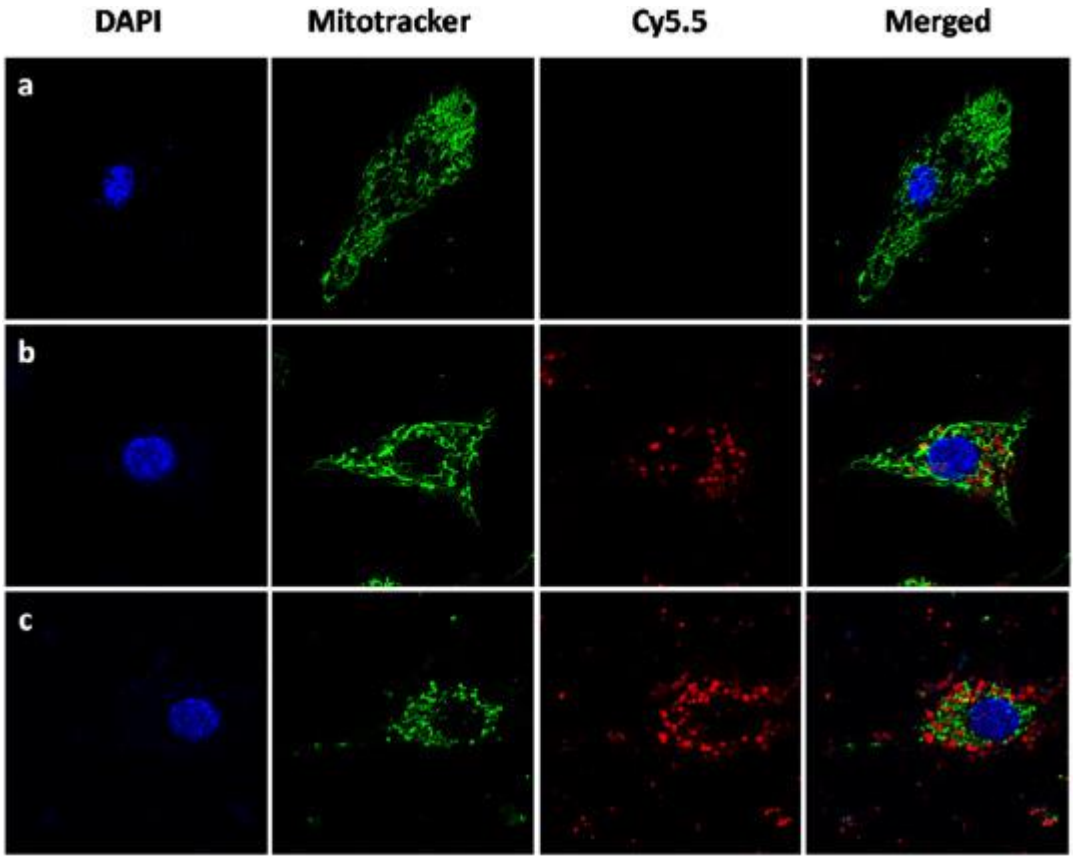

Fig. 6. Confocal microscope images of Human prostate cancer cell PC3. (a) Control nanoparticles; (b) 10 μg/mL TSPO targeted nanoparticles; (c) 20 μg/mL TSPO targeted nanoparticles. Blue: nucleus (DAPI), Green: mitochondria (MitoTracker™ Green FM), Red: TSPO targeted nanoparticles (Cy5.5).

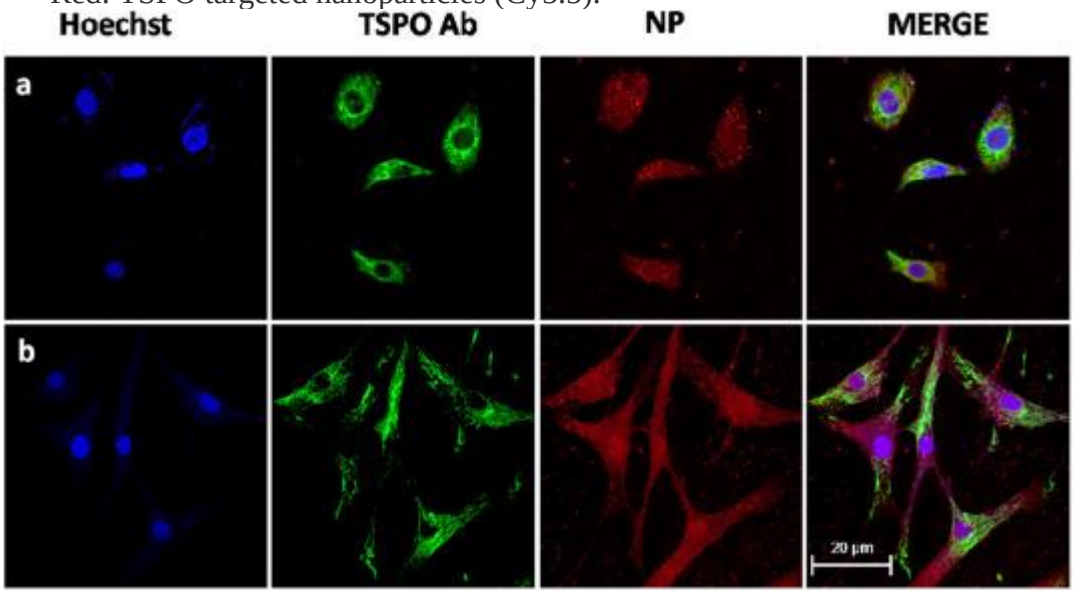

Fig. 7. Confocal microscope images of immunocytofluorescence. Comparison of two cell lines, prostate cancer cells and human fibroblast cells stained with nucleus staining dye

(blue, Hoechst), TSPO specific antibody (Green), and TSPO targeted nanoparticles (Red). (a) PC-3 (prostate cancer cells) as a positive control; (b) CCD-986sk (Human fibroblast cells) as a negative control.

A comparison of PC3 (Fig. 7a) and CCD-986sk (Fig. 7b) cells stained with TSPO specific antibody (Green), TSPO targeted nanoparticles (Red) and nucleus staining dye (blue) show a large merging area of red fluorescence of TSPO targeted nanoparticles with the green fluorescence of the TSPO antibody (Fig. 7a). Coherently this not occur in the negative model CCD-986sk (Fig. 7b) where red and green did not overlap.

The targeting ability of TSPO targeted nanoaprticles was confirmed measuring iron content *via* ICP-MS analysis. The data reported in Table 1 clearly show the higher accumulation of Fe in U87-MG and PC3 cells treated with TSPO targeted nanoparticles respect to those treated with not targeted nanoparticles, both after 4 and 24 h exposure.

Table 1. Iron content determined by ICP-MS analysis.

Time exposure	**Iron content (μg/L)**			
	U87-MG cells		**PC3 cells**	
	Targeted-NPs	**Not-targeted**	**Targeted-NPs**	**Not-targeted**
4 h	1200 ± 30	200 ± 15	900 ± 20	250 ± 8
24 h	900 ± 10	100 ± 7	800 ± 15	170 ± 10

Moreover, in order to assess the correlation between inflammatory responses and TSPO expression at a cellular level, U87-MG and PC3 cell were visualized after overnight incubation with lipopolysaccharide (LPS) before the treatment with TSPO-targeted nanoparticles. Immunocytofluorescent staining images reported in Fig. 8 show the overlap of red fluorescence of nanoparticles with the green one of TSPO antibody. Thus, in inflammatory states TSPO resulted expressed and TSPO targeted nanoparticles were able to recognize it.

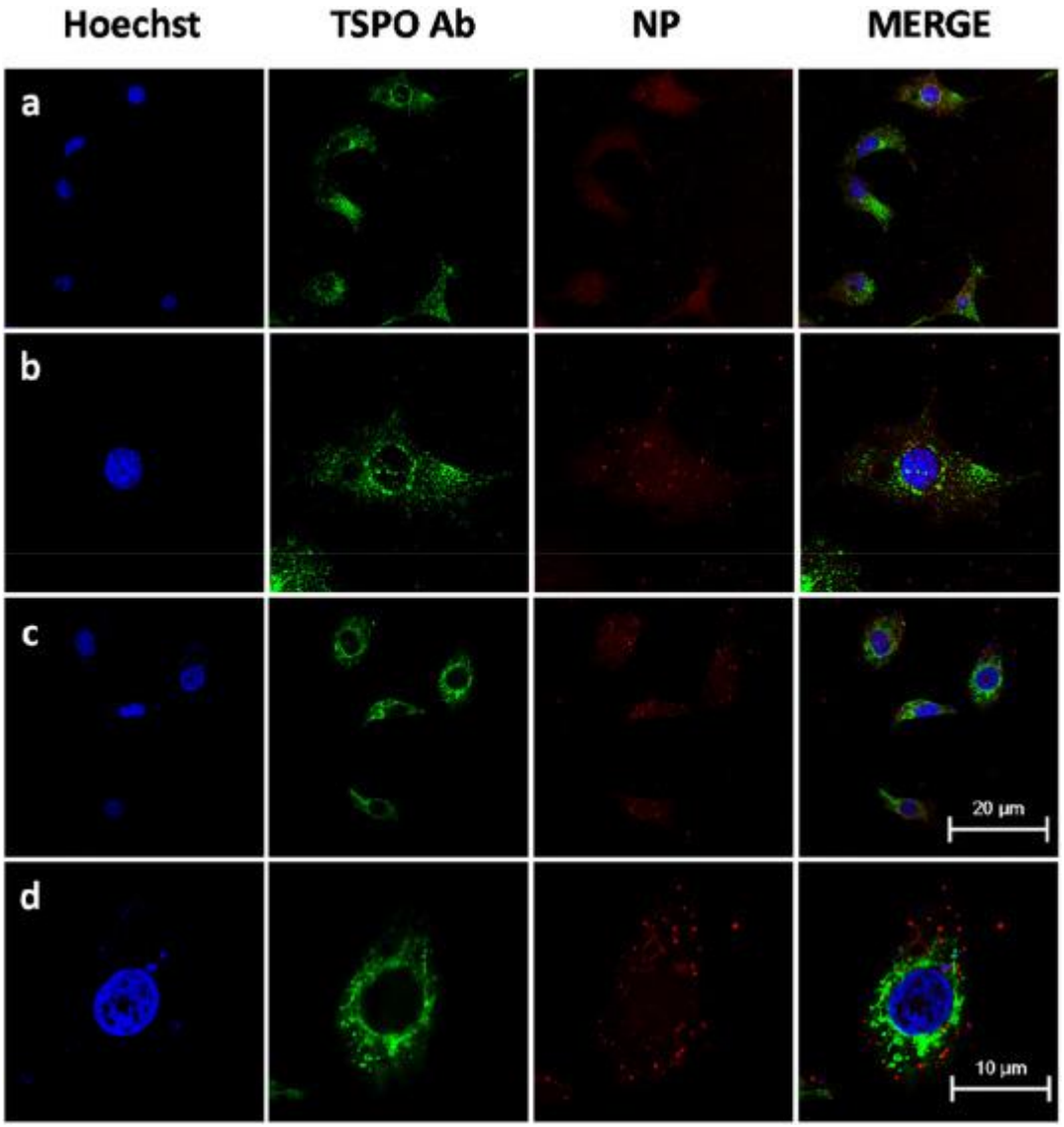

Fig. 8. Confocal microscope images of immunocytofluorescence from human glioblastoma U87-MG (a, b) and prostate cancer PC3 cells (c, d) stained with TSPO targeted nanoparticles at concentration 20 µg/mL (red) after overnight incubation with LPS 1 µg/mL. Blue: Nucleus (Hoechst), Green: TSPO (TSPO antibody), Red: TSPO-targeted nanoparticles. b and d images were enlarged from main images (2× a and c, respectively).

3.4. Small animal fluorescence images

After a preliminary *in vitro* evaluation of the ability of USPIOs-TSPO targeted nanoparticles to recognize the intracellular receptor TSPO, we performed *in vivo* experiments on U87-MG xenograft models obtained from 6-week-old male

Balb/c athymic mice, in order to assess their ability as new fluorescence imaging agents of GBM. The images in Fig. 9 obtained with IVIS®Lumina XRMS images set filter after inoculation of the control nanoparticles (Fig. 9a) or of TSPO targeted nanoparticles (Fig. 9b) show a marked increase of fluorescence intensity in the tumor area when the targeted nanoparticles were used. This signal also decays more slowly than that generated by the control nanoparticles.

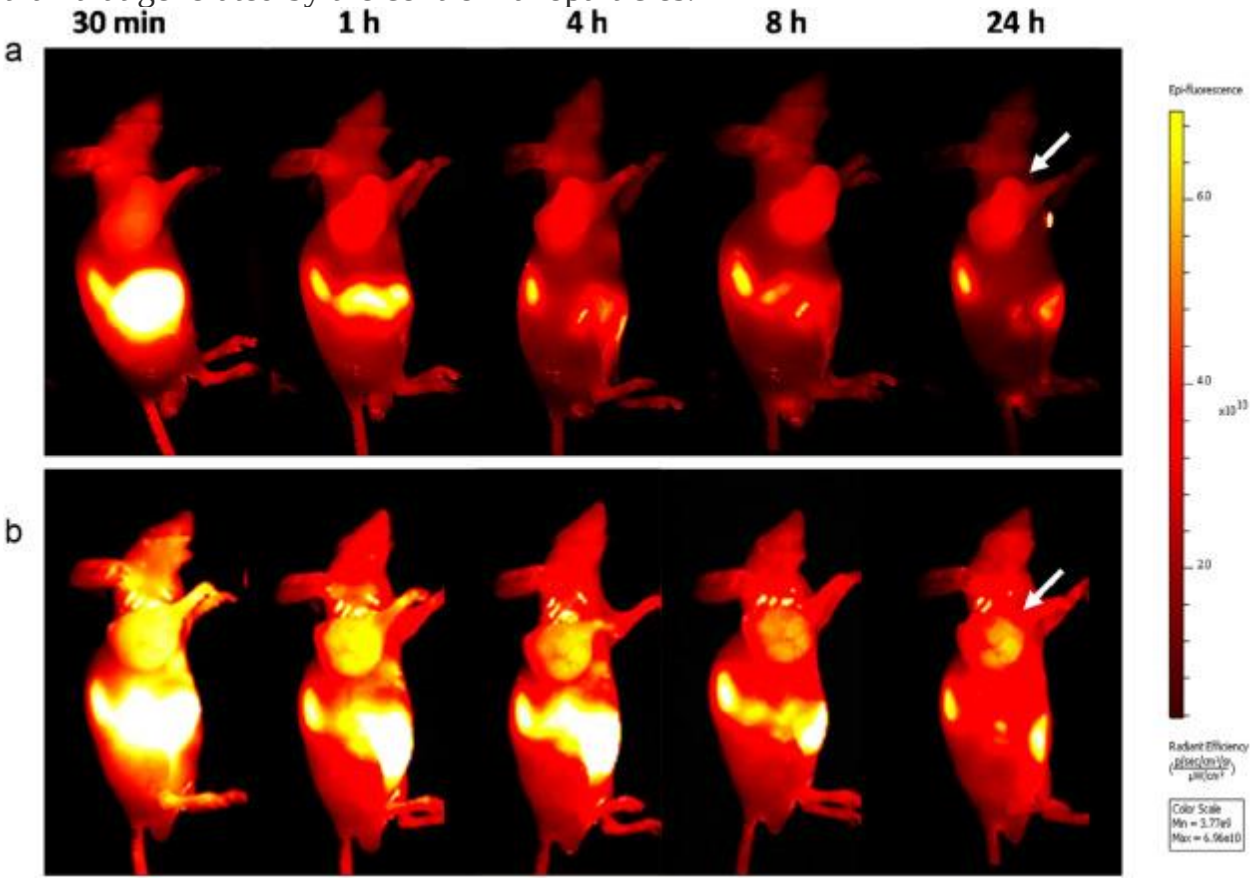

Fig. 9. (a) *In vivo* imaging after intravenous injection of 200 μg control nanoparticles (without conjugated TSPO ligand) at different time points from 30 min to 24 h post injection. (b) *In vivo* imaging after intravenous injection of 200 μg TSPO targeted nanoparticles at different time points from 30 min to 24 h post injection. The instrument used was IVIS®Lumina XRMS images set filter. Excitation filter = 660 nm, Emission filter = 710 nm. All fluorescence images had identical exposure times and same overall contrast settings to measure relative intensity difference.

In addition, a displacement experiment was carried out *in vivo* by pre-injecting the TSPO selective ligand PK 11195 before proceeding with the administration of the TSPO targeted-USPIOs nanoparticles. As shown in Fig. 10, the signal associated with the targeted nanoparticles, for every time post injection considered, was much more

intense in the absence of PK 11195 (Fig. 10a) than in the presence (Fig. 10b). These data were represented in a graph reported in Fig. 10c as a tumor-to-skin-ratio, from which the displacement capacity of PK 11195 by TSPO targeted-USPIOs nanoparticles was quantitatively demonstrated. This also confirmed the ability of the new prepared imaging nanosystem to reach *in vivo* the tumor target site. Moreover, in Fig. 11, are reported the organs distributions of TSPO targeted nanoparticles in both conditions mentioned above. The intravenous injected nanoparticles could be accumulated in the liver after mixing with the bile followed by excreting into the gastrointestinal tract (Vasquez et al., 2011; Zhang et al., 2016). We believe that our macromolecules (Cy5.5-TSPO ligand conjugated nanoparticle) are available to follow the same metabolic pathway in the living animal. The images in Fig. 11 clearly show a preferential distribution of nanoparticles at the tumor site.

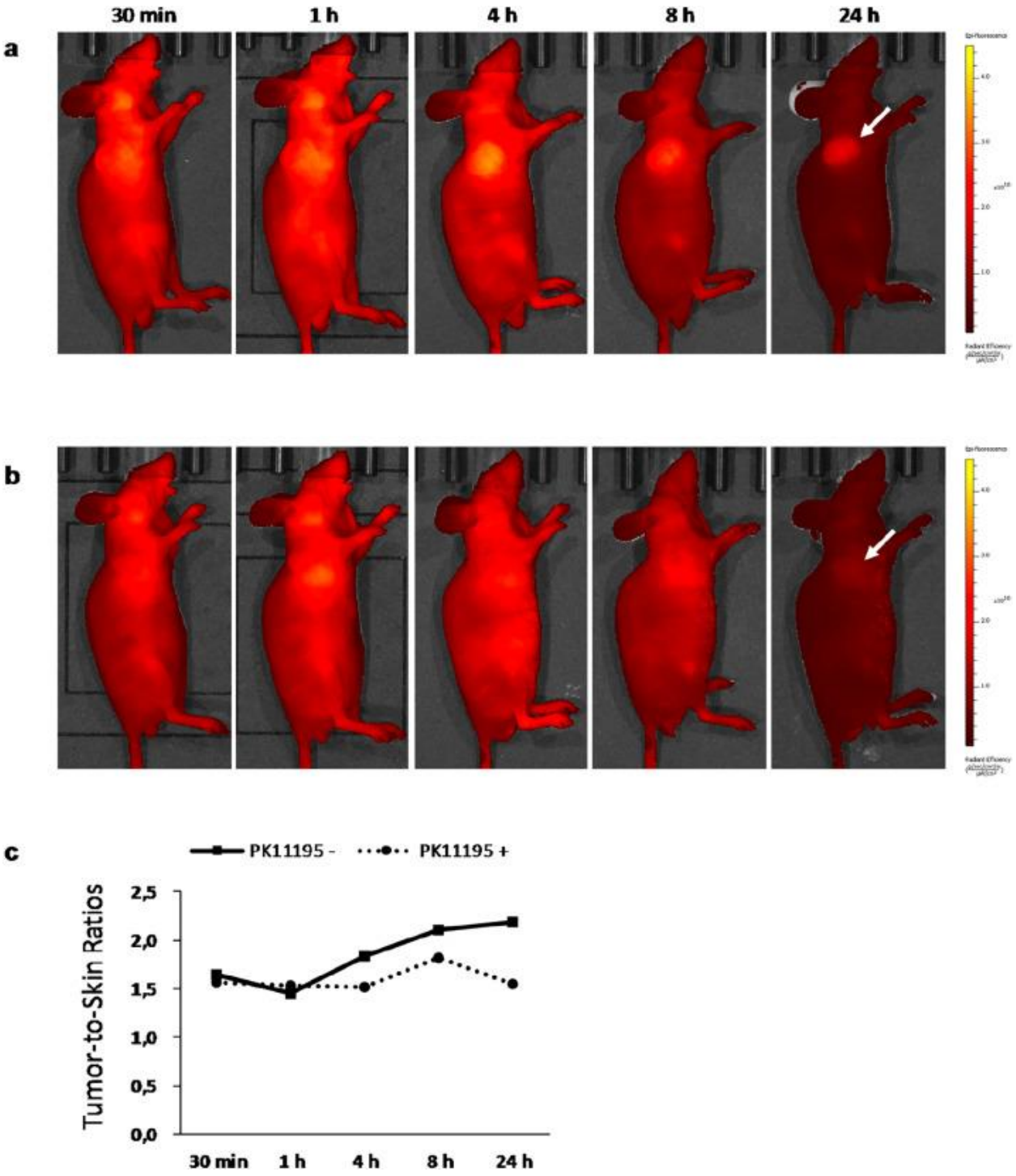

Fig. 10. Fluorescence imaging study by IVIS Lumina XRMS. (a) Imaging of U87-MG xenograft model at 30 min, 1 h, 4 h, 8 h, and 24 h post-injection of TSPO-targeted nanoparticle of 200 μg. (b) Inhibition study using PK 11195 (10 mg/1 kg). (c) Tumor-to-skin ratios in mouse models with PK 11195 pre-injection or without PK 11195 pre-injection.

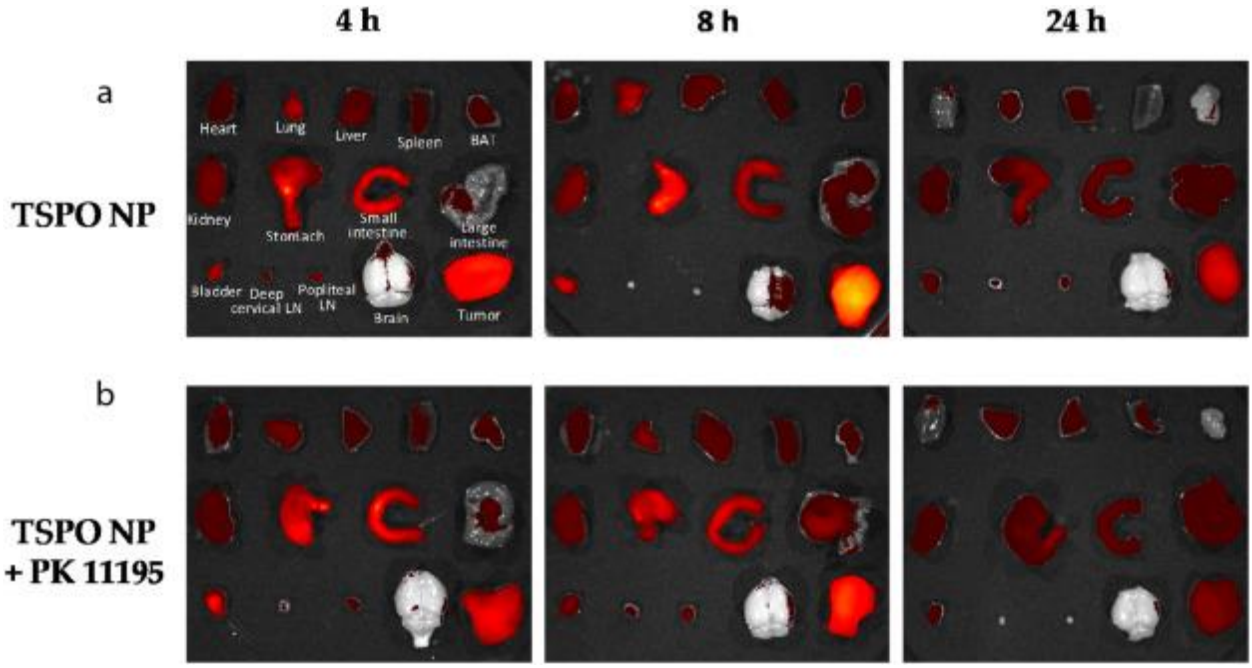

Fig. 11. Fluorescence imaging study by IVIS Lumina XRMS. (a) Imaging of organ distribution of TSPO-targeted nanoparticle in U87-MG xenograft model at 4 h, 8 h, and 24 h post-injection. (b) Organs distribution after inhibition study using PK 11195 (10 mg/1 kg).

4. Conclusions

The water-dispersible ultra-small iron oxide nanoparticles (USPIONs) were synthesized in one step and conjugated with Cyanine 5.5, a near-infrared fluorescent dye, and with a selective TSPO ligand in order to realize a new NIR emitting USPIOs-TSPO targeted nanosystem useful as an *in vivo* tool for fluorescence imaging of GBM. A broad evaluation of the optical and structural characteristics of the new TSPO targeted imaging nanosystem, confirmed the high colloidal stability in physiological media and the ability to preserve the relevant optical properties in the NIR region even after conjugation of the USPIONs with the TSPO ligand. The confocal microscopy investigation confirmed the cell internalization of the TSPO targeted-USPIONs and their selectivity for the TSPO receptor in all the TSPO over expressing cell lines. The ability to recognize the intracellular receptor was confirmed *in vitro* and *in vivo* by competition studies with the selective TSPO ligand PK 11195. Moreover, the images of U87-MG xenograft models administered with TSPO-USPIONs and acquired with X-ray multi-species optical imaging system

evidenced their effectiveness in the visualization of the tumor site. Thus, the proposed novel imaging system holds great promise as an optical TSPO targeted nanoprobe for *in vivo* NIR molecular imaging applications.

Author contributions

B.C.L. and Y.P. conceived and designed the experiment; C.L., J.Y.C., R.M.I, A.L., J.S.Y., I.H.S. and performed the synthesis, cell experiments, and fluorescence imaging experiments; J.S.Y. and S.E.K. analyzed the data; N.D., F.L, C.L., and B.C.L. wrote the paper.

Acknowledgments

This study was funded by the Ministry of Health and Welfare, the Seoul National University Bundang Hospital Research, and the National Research Foundation grant (HI16C0947, 14-2017-015, NRF-2018M2A2B3A02071842 and NRF-2017R1A2A2A05001433). The University of Bari "Aldo Moro" (Italy) and the Inter-University Consortium for Research on the Chemistry of Metal Ions in Biological Systems (C.I.R.C.M.S.B.) are also gratefully acknowledge for their financial support.

Declaration of competing interest

The authors declare no conflict of interest.

References

Cassano et al., 2017
T. Cassano, A. Lopalco, M. De Candia, V. Laquintana, A. Lopedota, A. Cutrignelli, M. Perrone, R.M. Iacobazzi, G. Bedse, M. Franco, N. Denora, C.D. Altomare

Oxazepam-dopamine conjugates increase dopamine delivery into striatum of intact rats
Mol. Pharm., 14 (2017), pp. 3178-3187, 10.1021/acs.molpharmaceut.7b00405
Choi et al., 2016
J.Y. Choi, R.M. Iacobazzi, M. Perrone, N. Margiotta, A. Cutrignelli, J.H. Jung, D.D. Park, B.S. Moon, N. Denora, S.E. Kim, B.C. Lee

Synthesis and evaluation of tricarbonyl ^{99m}Tc-labeled 2-(4-chloro)phenyl-imidazo[1,2-a] pyridine analogs as novel SPECT imaging radiotracer for TSPO-rich cancer

Int. J. Mol. Sci., 17 (2016), 10.3390/ijms17071085

Denora et al., 2008

N. Denora, V. Laquintana, M.G. Pisu, R. Dore, L. Murru, A. Latrofa, G. Trapani, E. Sanna

2-Phenyl-imidazo[1,2-a]pyridine compounds containing hydrophilic groups as potent and selective ligands for peripheral benzodiazepine receptors: Synthesis, binding affinity and electrophysiological studies

J. Med. Chem., 51 (2008), pp. 6876-6888, 10.1021/jm8006728

Denora et al., 2013

N. Denora, V. Laquintana, A. Lopalco, R.M. Iacobazzi, A. Lopedota, A. Cutrignelli, G. Iacobellis, C. Annese, M. Cascione, S. Leporatti, M. Franco

In vitro targeting and imaging the translocator protein TSPO 18-kDa through G(4)-PAMAM-FITC labeled dendrimer

J. Control. Release, 172 (2013), pp. 1111-1125, 10.1016/j.jconrel.2013.09.024

Denora et al., 2017

N. Denora, R.M. Iacobazzi, G. Natile, N. Margiotta

Metal complexes targeting the Translocator Protein 18 kDa (TSPO)

Coord. Chem. Rev., 341 (2017), pp. 1-18, 10.1016/j.ccr.2017.03.023

Depalo et al., 2017

Nicoletta Depalo, R.M. Iacobazzi, G. Valente, I. Arduino, S. Villa, F. Canepa, V. Laquintana, E. Fanizza, M. Striccoli, A. Cutrignelli, A. Lopedota, L. Porcelli, A. Azzariti, M. Franco, M.L. Curri, N. Denora

Sorafenib delivery nanoplatform based on superparamagnetic iron oxide nanoparticles magnetically targets hepatocellular carcinoma

Nano Res., 10 (2017), pp. 2431-2448, 10.1007/s12274-017-1444-3

Depalo et al., 2017a

N. Depalo, M. Corricelli, I. De Paola, G. Valente, R.M. Iacobazzi, E. Altamura, D. Debellis, D. Comegna, E. Fanizza, N. Denora, V. Laquintana, F. Mavelli, M. Striccoli, M. Saviano, A. Agostiano, A. Del Gatto, L. Zaccaro, M.L. Curri

NIR emitting nanoprobes based on cyclic RGD motif conjugated PbS quantum dots for integrin-targeted optical bioimaging

ACS Appl. Mater. Interfaces, 9 (2017), 10.1021/acsami.7b14155

Depalo et al., 2017b

N. Depalo, R.M. Iacobazzi, G. Valente, I. Arduino, S. Villa, F. Canepa, V. Laquintana, E. Fanizza, M. Striccoli, A. Cutrignelli, A. Lopedota, L. Porcelli, A. Azzariti, M. Franco, M.L. Curri, N. Denora

Sorafenib delivery nanoplatform based on superparamagnetic iron oxide nanoparticles magnetically targets hepatocellular carcinoma
Nano Res., 10 (2017), 10.1007/s12274-017-1444-3

Elkamhawy et al., 2015
A. Elkamhawy, A.N.I. Viswanath, A.N. Pae, H.Y. Kim, J.C. Heo, W.K. Park, C.O. Lee, H. Yang, K.H. Kim, D.H. Nam, H.J. Seol, H. Cho, E.J. Roh

Discovery of potent and selective cytotoxic activity of new quinazoline-ureas against TMZ-resistant glioblastoma multiforme (GBM)
Eur. J. Med. Chem., 103 (2015), pp. 210-222, 10.1016/j.ejmech.2015.08.001

Fanizza et al., 2016a
E. Fanizza, R.M. Iacobazzi, V. Laquintana, G. Valente, G. Caliandro, M. Striccoli, A. Ag ostiano, A. Cutrignelli, A. Lopedota, M.L. Curri, M. Franco, N. Depalo, N. Denora

Highly selective luminescent nanostructures for mitochondrial imaging and targeting
Nanoscale, 8 (2016), pp. 3350-3361, 10.1039/c5nr08139d

Fanizza et al., 2016b
E. Fanizza, R.M. Iacobazzi, V. Laquintana, G. Valente, G. Caliandro, M. Striccoli, A. Ag ostiano, A. Cutrignelli, A. Lopedota, M.L. Curri, M. Franco, N. Depalo, N. Denora

Highly selective luminescent nanostructures for mitochondrial imaging and targeting
Nanoscale, 8 (2016), 10.1039/c5nr08139d

Halamoda Kenzaoui et al., 2013
B. Halamoda Kenzaoui, S. Angeloni, T. Overstolz, P. Niedermann, C. Chapuis Bernasconi, M. Liley, L. Juillerat-Jeanneret

Transfer of ultrasmall iron oxide nanoparticles from human brain-derived endothelial cells to human glioblastoma cells
ACS Appl. Mater. Interfaces, 5 (2013), pp. 3581-3586, 10.1021/am401310s

Iacobazzi et al., 2017
R.M. Iacobazzi, P. Letizia, L.A. Assunta, L. Valentino, L. Antonio, C. Annalisa, A. Emili ano, D.F. Roberta, A. Amalia, F. Massimo, D. Nunzio

Targeting human liver cancer cells with lactobionic acid-G(4)-PAMAM-FITC sorafenib loaded dendrimers
Int. J. Pharm., 528 (2017), 10.1016/j.ijpharm.2017.06.049
Iacobazzi et al., 2017a

Rosa
Maria Iacobazzi, P. Letizia, L.A. Assunta, L. Valentino, L. Antonio, C. Annalisa, A. Emiliano, D.F. Roberta, A. Amalia, F. Massimo, D. Nunzio

Targeting human liver cancer cells with lactobionic acid-G(4)-PAMAM-FITC sorafenib loaded dendrimers
Int. J. Pharm., 528 (2017), pp. 485-497, 10.1016/j.ijpharm.2017.06.049
Iacobazzi et al., 2017b
R.M. Iacobazzi, A. Lopalco, A. Cutrignelli, V. Laquintana, A. Lopedota, M. Franco, N. Denora

Bridging pharmaceutical chemistry with drug and nanoparticle targeting to investigate the role of the 18-kDa translocator protein TSPO
ChemMedChem, 12 (2017), pp. 1261-1274, 10.1002/cmdc.201700322
Laquintana et al., 2016
V. Laquintana, N. Denora, A. Cutrignelli, M. Perrone, R. Iacobazzi, C. Annese, A. Lopalco, A. Lopedota, M. Franco

TSPO ligand-methotrexate prodrug conjugates: design, synthesis, and biological evaluation
Int. J. Mol. Sci., 17 (2016), 10.3390/ijms17060967
Lopalco and Denora, 2018
A. Lopalco, N. Denora

Nanoformulations for drug delivery: safety, toxicity, and efficacy
Methods Mol. Biol., 1800 (2018), pp. 347-365, 10.1007/978-1-4939-7899-1_17
Lopalco et al., 2015
A. Lopalco, H. Ali, N. Denora, E. Rytting

Oxcarbazepine-loaded polymeric nanoparticles: development and permeability studies across in vitro models of the blood–brain barrier and human placental trophoblast
Int. J. Nanomedicine, 10 (2015), pp. 1985-1996, 10.2147/IJN.S77498
Lopalco et al., 2018
A. Lopalco, A. Cutrignelli, N. Denora, M. Perrone, R.M. Iacobazzi, E. Fanizza, A. Lopedota, N. Depalo, M. De Candia, M. Franco, V. Laquintana

Delivery of proapoptotic agents in glioma cell lines by TSPO ligand–dextran nanogels
Int. J. Mol. Sci., 19 (2018), 10.3390/ijms19041155
Mangiatordi et al., 2017
G.F. Mangiatordi, D. Trisciuzzi, D. Alberga, N. Denora, R.M. Iacobazzi, D. Gadaleta, M. Catto, O. Nicolotti

Novel chemotypes targeting tubulin at the colchicine binding site and unbiasing P-glycoprotein
Eur. J. Med. Chem., 139 (2017), pp. 792-803, 10.1016/j.ejmech.2017.07.037

Midzak et al., 2015
A. Midzak, N. Denora, V. Laquintana, A. Cutrignelli, A. Lopedota, M. Franco, C.D. Alto mare, V. Papadopoulos

2-Phenylimidazo[1,2-a]pyridine-containing ligands of the 18-kDa translocator protein (TSPO) behave as agonists and antagonists of steroidogenesis in a mouse leydig tumor cell line
Eur. J. Pharm. Sci., 76 (2015), pp. 231-237, 10.1016/j.ejps.2015.05.021

M. Perrone, B.S. Moon, H.S. Park, V. Laquintana, J.H. Jung, A. Cutrignelli, A. Lopedota, M. Franco, S.E. Kim, B.C. Lee, N. Denora

A novel PET imaging probe for the detection and monitoring of translocator protein 18 kDa expression in pathological disorders
Sci. Rep., 6 (2016), 10.1038/srep20422
Piccinonna et al., 2012
S. Piccinonna, N. Margiotta, C. Pacifico, A. Lopalco, N. Denora, S. Fedi, M. Corsini, G. Natile

Dinuclear Pt (II)-bisphosphonate complexes: a scaffold for multinuclear or different oxidation state platinum drugs
Dalt. Trans., 41 (2012), pp. 9689-9699, 10.1039/c2dt30712j
Piccinonna et al., 2013
S. Piccinonna, N. Margiotta, N. Denora, R.M. Iacobazzi, C. Pacifico, G. Trapani, G. Natil e

A model radiopharmaceutical agent targeted to translocator protein 18 kDa (TSPO)
Dalt. Trans., 42 (2013), Article 10112, 10.1039/c3dt51152a
Savino et al., 2016
S. Savino, N. Denora, R. Iacobazzi, L. Porcelli, A. Azzariti, G. Natile, N. Margiotta

Synthesis, characterization, and cytotoxicity of the first oxaliplatin Pt (IV) derivative having a TSPO ligand in the axial position
Int. J. Mol. Sci., 17 (2016), p. 1010, 10.3390/ijms17071010
Stupp et al., 2009
R. Stupp, M.E. Hegi, W.P. Mason, M.J. van den
Bent, M.J. Taphoorn, R.C. Janzer, S.K. Ludwin, A. Allgeier, B. Fisher, K. Belanger, P. H au, A.A. Brandes, J. Gijtenbeek, C. Marosi, C.J. Vecht, K. Mokhtari, P. Wesseling, S. Vil la, E. Eisenhauer, T. Gorlia, M. Weller, D. Lacombe, J.G. Cairncross, R.-O. Mirimanoff

Effects of radiotherapy with concomitant and adjuvant temozolomide versus radiotherapy alone on survival in glioblastoma in a randomised phase III study: 5-year analysis of the EORTC-NCIC trial
Lancet Oncol, 10 (2009), pp. 459-466, 10.1016/S1470-2045(09)70025-7
Vasquez et al., 2011
K.O. Vasquez, C. Casavant, J.D. Peterson

Quantitative whole body biodistribution of fluorescent-labeled agents by non-invasive tomographic imaging
PLoS One, 6 (2011), Article e20594, 10.1371/journal.pone.0020594
Yang et al., 2014
K.M. Yang, H. Il Cho, H.J. Choi, Y. Piao

Synthesis of water well-dispersed PEGylated iron oxide nanoparticles for MR/optical lymph node imaging
J. Mater. Chem. B, 2 (2014), pp. 3355-3364, 10.1039/c4tb00084f
Zhang et al., 2016
Y.-N. Zhang, W. Poon, A.J. Tavares, I.D. McGilvray, W.C.W. Chan

Nanoparticle–liver interactions: cellular uptake and hepatobiliary elimination
J. Control. Release, 240 (2016), pp. 332-348, 10.1016/j.jconrel.2016.01.020

[1]

These authors contributed equally to this work.